AIAA JOURNAL
Vol. 40, No. 1, January 2002

# Turbulence Ingestion Noise, Part 1: Experimental Characterization of Grid-Generated Turbulence

John P. Wojno* and Thomas J. Mueller†
*University of Notre Dame, Notre Dame, Indiana 46556*
and
William K. Blake‡
*U.S. Naval Surface Warfare Center, West Bethesda, Maryland 20817-5700*

**Results are presented of an experimental investigation into the aeroacoustic response characteristics of rotor turbulence ingestion. To fully characterize the rotor response, both the ingested velocity field and the resulting far-field sound were measured. The results are presented of a detailed velocity characterization, which was performed upstream of the rotor. The velocity measurements included an evaluation of the streamwise development of turbulence characteristics downstream of the grid, a high-resolution mapping of the spatial distribution of the mean velocity and rms turbulence fluctuations in the rotor inlet plane, and the development of a semi-empirical, functional representation of the three-dimensional wave number spectral density of the ingested turbulence. These data comprise a comprehensive empirical velocity model that was developed for specific application to rotor turbulence ingestion noise (Wojno, J. P., Mueller, T. J., and Blake, W. K., "Turbulence Ingestion Noise, Part 2: Rotor Aeroacoustic Response to Grid-Generated Turbulence," *AIAA Journal*, Vol. 40, No. 1, 2002, pp. 26–32).**

## Nomenclature

| | | |
|---|---|---|
| $\hat{a}$ | = | empirically determined constant used to define streamwise wave number model |
| $a_i, b_i, c_i$ | = | empirically determined constants used to define quadratic, cross-stream wave number model in the $i$th direction |
| $B$ | = | number of rotor blades |
| $d$ | = | rod diameter of turbulence generation grid |
| $E(k_1)$ | = | nondimensional, streamwise wave number spectral density of turbulence (in the manner of von Kármán) |
| $f$ | = | temporal frequency |
| $G(f)$ | = | unsteady aerodynamic response function |
| $g(r)$ | = | lateral velocity correlation function |
| $H(f)$ | = | acoustic propagation model |
| $J$ | = | rotor advance ratio |
| $\boldsymbol{k}$ | = | wave vector |
| $k_e$ | = | wave number of the energy containing eddies (from isotropic turbulence theory) |
| $k_1$ | = | streamwise wave number |
| $k_2$ | = | wave number normal to the blade |
| $k_{12}$ | = | composite wave number along rotation direction |
| $L_R$ | = | rotor blade span (defined from hub to tip) |
| $M$ | = | Mach number |
| $m$ | = | mesh spacing of turbulence generation grid |
| $n$ | = | circumferential harmonic mode number of mean velocity field |
| $R$ | = | radial location in the rotor inlet plane |
| $R_{uu}(\boldsymbol{x}, t)$ | = | nondimensional, two-point, velocity correlation function at time $t$ |
| $S_{ab}(\boldsymbol{x}, f)$ | = | two-sided, temporal cross spectrum between sensors located at $a$ and $b = a + \boldsymbol{x}$ |
| $s_{\text{grid}}$ | = | solidity of turbulence generation grid |
| $U(R, \phi)$ | = | measured mean flow velocity at $(R, \phi)$, in the rotor inlet plane |
| $U_0(R)$ | = | resultant mean flow velocity (in the rotating reference frame) |
| $U_\infty$ | = | freestream mean flow velocity |
| $\bar{U}^\phi(R)$ | = | circumferentially averaged mean flow velocity at radius $R$ |
| $u_i$ | = | velocity fluctuation in the $i$th direction |
| $\underline{u}_{\text{rms}}$ | = | rms turbulence fluctuation |
| $\overline{u^2}$ | = | mean-squared turbulence velocity |
| $V_c$ | = | convection velocity |
| $V(R, \phi)$ | = | variation of mean velocity field with respect to circumferential mean |
| $\tilde{V}(R_l, n)$ | = | discrete circumferential modes of the mean velocity field |
| $\boldsymbol{x}$ | = | sensor separation vector |
| $\gamma(\boldsymbol{x}, f)$ | = | nondimensional, cross-spectral density over separation $\boldsymbol{x}$ |
| $\gamma^2(\boldsymbol{x}, f)$ | = | coherence of signals measured over separation $\boldsymbol{x}$ |
| $\Delta R$ | = | radial step size of spatial velocity test grid |
| $\Delta r$ | = | discrete radial sensor separation increment |
| $\Delta\theta$ | = | discrete tangential sensor separation increment |
| $\Delta\phi$ | = | tangential step size of spatial velocity test grid |
| $\delta$ | = | Kronecker delta function |
| $\eta_i$ | = | cosine describing the $i$th direction |
| $\theta$ | = | relative tangential sensor separation distance |
| $\Lambda_i$ | = | turbulence length scale in $i$th direction |
| $\rho$ | = | fluid density |
| $\Phi_{pp}(f)$ | = | measured far-field acoustic spectrum |
| $\tilde{\Phi}_{pp}(f)$ | = | estimated far-field acoustic spectrum |
| $\Phi_{TT}(f)$ | = | rotor unsteady thrust spectrum |
| $\Phi_{uu}(\boldsymbol{k})$ | = | three-dimensional turbulent wave number spectrum |
| $\phi, \phi_n$ | = | tangential location in the rotor inlet plane |
| $\phi(k_i)$ | = | nondimensional, spectral density in the $i$th direction wave number domain |
| $\phi_{uu}(f)$ | = | temporal autospectral density of turbulence |

Received 6 December 1999; revision received 1 June 2001; accepted for publication 11 June 2001. 

*Research Assistant, Aerospace and Mechanical Engineering Department; currently Acoustic Engineer, Hydroacoustics, U.S. Naval Surface Warfare Center, Carderock Division, Code 7250, West Bethesda, MD 20817-5700.

†Roth-Gibson Professor, Aerospace and Mechanical Engineering Department. Associate Fellow AIAA.

‡Chief Scientist, Hydroacoustics, Carderock Division, Code 7023.

## I. Introduction

HISTORICALLY, rotor turbulence ingestion noise (TIN) has been studied by numerous investigators. Rather than give an exhaustive discussion of decades of scientific literature, only the highlights of particular studies, which were primary sources

of information throughout the course of the current research, are presented.

The current research project was a modern extension of the pioneering work of Sevik.[1] Sevik's paper outlined an analytic procedure for estimating the aeroacoustic response of a 10-bladed rotor, based on the two-point velocity correlation function, assuming isotropic turbulence. To support his analytic work, Sevik presented limited experimental data, consisting primarily of the power spectral density of the unsteady thrust. Far-field acoustic spectra were implied from the measured thrust data, assuming dipole radiation. Sevik's analytic model successfully captured the broadband portion of the response, but failed to predict an experimentally observed narrowband component about the blade passing frequency and higher harmonics.

In contrast to the spatial approach used by Sevik,[1] Blake defined a spectral analysis technique to estimate the rotor response in the temporal frequency and spatial wave number domains.[2] This approach defined the unsteady thrust response of the rotor in terms of the spectral content of the ingested turbulence field. Once the thrust spectrum was determined, the far-field acoustic propagation was defined in terms of dipole radiation, in the manner of Lighthill.[3,4] By the use of asymptotic expansions to define the degree of correlation, Blake[2] demonstrated the ability to recover either the purely broadband or narrowband portion of the response from the general formulation.

Martinez and Weissman[5] modified Sevik's correlation analysis[1] to predict the narrowband behavior of the propeller response. They[5] assumed the rotational velocity component to be dominant, which highly correlated the individual blade responses. This procedure recovered the narrowband response at the expense of the broadband component.

Recently, Martinez extended his analytic technique to more general functional forms of the velocity correlation function.[6–8] This theory was developed using asymptotic analyses for rotors with large numbers of blades ($B \geq 6$). The resulting analytic solution predicted both the narrow-band and broadband response components. In Ref. 6, Martinez demonstrated that the analysis captured the primary circumferential mode of Sevik's empirical data[1] very well. However, the theory significantly underpredicted the narrowband response at twice the blade passing frequency (BPF). In his discussion, Martinez suggested[6] that Sevik's[1] empirical response data may be suspect.

Another closely related project was the work of Paterson and Amiet.[9] They measured the acoustic response characteristics of a NACA-0012 airfoil subjected to grid-generated turbulence. The experimental analysis included a characterization of the turbulent inflow, as well as measurements of the local surface pressure on the airfoil and the far-field acoustic radiation. The measured turbulence characteristics included the nominal rms intensities of the axial and normal (defined with respect to the airfoil) turbulence components, nominal integral scales in both directions, the temporal autospectra of each turbulence component, and the spanwise cross spectrum of the vertical turbulence component as a function of the nondimensionalized spanwise separation distance. The temporal spectra were extended to the streamwise wave number domain using Taylor's hypothesis. These experimental results were compared to the corresponding theoretical values, generated using classical aerodynamic and aeroacoustic analysis techniques.

Finally, the current effort was similar to the recent research of Manoha.[10] In this work, the acoustic production of a propeller ingesting boundary-layer turbulence was experimentally investigated. A scaled propeller was mounted on the rear of an axisymmetric body. Detailed velocity correlation measurements were performed in all of the spatial directions of the cylindrical, body-fixed coordinate system. These correlation measurements were used to define the spectral content of the ingested turbulent velocity field. A numerical prediction model, based on the spectral techniques of Ffowcs-Williams and Hawkings,[11] was used to estimate the spectrum of the radiated acoustics in the far field. These estimates were compared to corresponding measured values. These data demonstrated both the broadband nature of the far-field acoustic spectrum, as well as a narrowband response, centered about the BPF and higher harmonics.

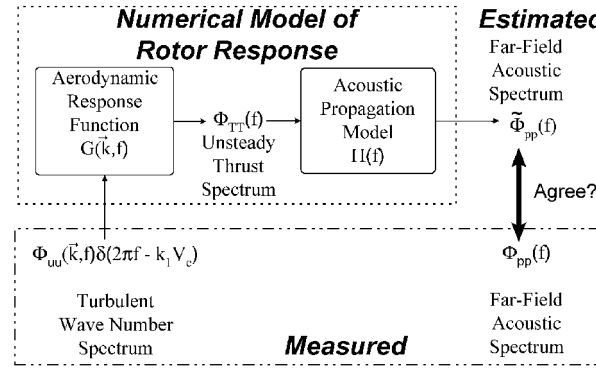


**Fig. 1 Functional block diagram of the comparisons between the predicted and measured responses.**

Rotor TIN has been a topic of investigation at Notre Dame. The work of Scharpf[12] and Minniti et al.[13] examined the aeroacoustic response characteristics of a four-bladed rotor to grid-generated turbulence. However, the velocity data in these studies were limited to the classical turbulence parameters, such as the rms turbulence intensity, the Lagrangian integral scale, and the temporal autospectrum.

The primary objective of the current research was to characterize empirically the ingested velocity field. To achieve this objective, a series of detailed velocity measurements was performed in the rotor inlet plane, to define both the large-scale spatial distribution of mean and fluctuating velocity components and a representative fine-scale turbulence spectrum, as experienced by a rotor blade sweeping through the flowfield. Additional velocity measurements were also made, at a series of streamwise locations, to determine the streamwise development of turbulence downstream of the grid. These tests included an experiment designed to evaluate the validity of Taylor's hypothesis at the rotor inlet plane.

Note that the motivation behind this research was to better understand the physical mechanisms responsible for rotor TIN. Physically, the rotor interaction with the temporally and spatially varying velocity field establishes an unsteady pressure distribution on the blades, which propagates away from the body to generate noise in the far field. This application drove the definition of each of the velocity tests, as outlined in Sec. III.

Furthermore, the detailed velocity characterization presented below is used in Part 2 of this paper[14] to estimate the broadband response of a 10 bladed rotor to the ingested turbulence field. These predictions are compared to corresponding measured data to assess the fidelity of the response model. The methodology for the assessment is graphically depicted in Fig. 1.

## II. Theoretical Development

This research focused on the broadband aeroacoustic response of a rotor ingesting the grid-generated turbulence field, and so the velocity characteristics of interest were primarily those needed to describe the ingested turbulence. A procedure for defining a semi-empirical, three-dimensional spectrum model of the small-scale turbulence, in terms of the measured velocity data, is presented in Sec. II.A. However, the rotor is also acoustically responsive to certain large-scale spatial inhomogeneities in the velocity field.[2,15] In particular, when the circumferential mode number of the spatial inhomgeneity is an integral multiple of the number of blades, the blade rotation generates pure tones at the rotor BPF and higher harmonics. Therefore, it was necessary to determine the circumferential modal composition of the mean velocity field in the rotor inlet plane. A discrete method of estimating the modal content, based on a discrete Fourier transform (DFT) technique, is developed in Sec. II.B. Because of space and time constraints, only the highlights of these analyses are presented here. Detailed derivations of the theoretical development are presented by Wojno.[15]

### A. Turbulence Model

The spectral density of the ingested turbulence in all three spatial directions was needed to estimate the rotor thrust response.[15] It was

not feasible to determine simultaneously the functional behavior of the turbulence spectral density with respect to all three spatial directions. Instead, it was assumed that the behavior in each of the directions was independent of the others. Consequently, the three-dimensional turbulence spectrum was modeled as the product of the mean-squared turbulence fluctuation, the nondimensional streamwise spectral density, and the nondimensional spectral densities in each of the cross-stream spatial directions:

$$\Phi_{uu}(\boldsymbol{k}) = \overline{u^2}\phi(k_1)\phi(k_r)\phi(k_\theta) \tag{1}$$

Physically, Eq. (1) can be interpreted as follows. The mean-squared turbulence fluctuation defines the overall energy level of the ingested turbulence field $\overline{u^2}$. The streamwise spectral density $\phi(k_1)$ defines the energy distribution with respect to streamwise scales (or, equivalently, temporal frequency). The two cross-stream spectral densities, $\phi(k_r)$ and $\phi(k_\theta)$, operate on this energy density to account for spatial correlation decay in the radial and tangential directions, respectively. Thus, it was necessary to devise a method to estimate empirically each of the required spectral density functions. Equation (1) formed the basis of the semi-empirical turbulence model that was developed to predict rotor TIN.[15]

*Streamwise Spectral Density Function*

As noted in Eq. (1), the essential energy distribution of the turbulence spectrum is captured by the autospectral density of the turbulence velocity in the streamwise direction. However, if the convection velocity is significantly larger than the turbulent fluctuations, or, equivalently, the streamwise turbulence scale is significantly larger than the corresponding cross-stream scales, convection is the dominant temporal feature of the flowfield.[16] This assumption is known as Taylor's hypothesis, and it can be written symbolically as follows:

$$\frac{\partial}{\partial t} = \frac{\partial}{\partial x_1}\frac{\partial x_1}{\partial t} \approx V_c\frac{\partial}{\partial x_1}$$

Therefore, the streamwise autospectral density is related via the local convection velocity $V_c$ to the temporal autospectral density at a given location:

$$\phi(k_1) = \phi_{uu}(f)\delta(2\pi f - k_1 V_c) \tag{2}$$

Note that the definition of the local convection velocity $V_c$ changes with reference frame. In the inertial, cylindrical reference frame in which the turbulent velocity measurements were made, the appropriate convection speed was simply the freestream flow velocity $U_\infty$. However, in the rotating, blade-fixed reference frame, in which the unsteady aerodynamic response analysis was performed,[14,15] the convection velocity also includes the linear velocity component associated with the rotational motion of the local blade section. However, transformation into the streamwise wave number domain ensures proper implementation because $k_1$ is also based on the local convection velocity, as follows:

$$k_1 = 2\pi f / V_c \tag{3}$$

$$V_c(R) \equiv U_0(R) = \sqrt{U_\infty^2 + (\Omega R)^2} \tag{4}$$

Taylor's hypothesis is conveniently used in weak turbulence applications ($u_{\text{rms}}/U \leq 0.1$). It will be shown in Sec. IV.A, that this criterion applies to the current research. Consequently, Taylor's hypothesis was used to define the streamwise spectral density in the empirical turbulence model in terms of the measured temporal autospectral density of the turbulent velocity. However, additional tests were performed to evaluate the fidelity of this approximation. Based on the measured cross-spectral density of turbulence measured over streamwise specified separations, the streamwise scales were empirically estimated, using the analysis techniques to be presented. These data are compared to the corresponding cross-stream scales in Sec. IV.C to evaluate the validity of Taylor's hypothesis.

*Two-Point Velocity Correlations*

To assess the spatial correlation decay, an exponentially decaying velocity correlation model was used. According to this model, the velocity correlation over a defined spatial separation $\boldsymbol{x}$ at a given time $t$, can be approximated as follows:

$$R_{uu}(\boldsymbol{x}, t) \equiv \overline{u(\boldsymbol{x}_0, t)u(\boldsymbol{x}_1, t)}/\overline{u^2} \approx \exp[-|\boldsymbol{x}|/\Lambda_x(t)] \tag{5}$$

Because the only time-dependent parameters are the velocity correlation function and the integral turbulence scale, a Fourier transform can be applied to Eq. (5). This yields an equivalent spectral equation, which relates the measured nondimensional, cross-spectral density of turbulent velocities $\gamma(\boldsymbol{x}, f)$ over a given separation $\boldsymbol{x}$ to a frequency-dependent turbulence scale $\Lambda_x(f)$. Note that the nondimensional, cross-spectral density is simply the square root of the coherence between the turbulence velocities at the two locations:

$$\gamma(\boldsymbol{x}, f) \equiv \sqrt{\gamma^2(\boldsymbol{x}, f)} = \left[\frac{S_{01}(\boldsymbol{x}, f)S_{01}^*(\boldsymbol{x}, f)}{S_{00}(f)S_{11}(f)}\right]^{\frac{1}{2}} \approx \exp\left[-\frac{|\boldsymbol{x}|}{\Lambda_x(f)}\right] \tag{6}$$

This model was directly inverted to estimate empirically the turbulence scales in each direction using the measured cross-spectral density data over specific separation distances.

*Cross-Stream Spectral Density Functions*

The nondimensional, radial and tangential spectral density functions required for Eq. (1) were obtained by applying a spatial Fourier transformation to the exponential decay prescribed by Eq. (6) into the corresponding wave number domain. The resulting spectral density function, presented in generalized form, which accounts for the correlation decay in the $x_i$ direction, is given by

$$\phi(k_i) \equiv \phi(f, k_i) = [\Lambda_i(f)/\pi]\left\{1\Big/\left[1 + k_i^2\Lambda_i^2(f)\right]\right\} \tag{7}$$

This theoretical form of the cross-stream turbulent spectral density function was used to define the decay with respect to the radial and tangential directions in the semi-empirical three-dimensional turbulence spectrum model defined in Eq. (1). However, an estimate of the turbulence integral scale in each of the cross-stream directions was required to substitute into Eq. (7).

*Spatial Turbulence Scales*

Empirical estimates of the cross-stream turbulence scales were approximated by inverting Eq. (6). When the flow is assumed convection dominated, the streamwise wave number is equivalent to the temporal frequency. Consequently, Taylor's hypothesis was used to transform the frequency dependence of the scales to a streamwise wave number dependence, as shown in Eq. (2). However, the empirical data were necessarily discrete functions of both temporal frequency and separation distance. This discrete nature limited their validity to similar parameter step sizes. To avoid these inherent limitations, continuous functions were fitted to the discrete empirical scale estimates.

The resulting functional approximation was similar to one used by Corcos to model pressure correlations in a turbulent boundary layer.[17] Corcos defined a frequency-dependent turbulence scale model $\Lambda$ that was inversely proportional to the streamwise wave number,

$$\Lambda \approx \hat{a}/k_1 \tag{8}$$

However, Corcos's[17] model tends toward an infinite scale as the temporal frequency approaches zero. Physically, this requires that the correlation go identically to unity at the steady state, which did not agree with the measured cross-stream data. Furthermore, the inverse linear wave number dependence did not decay rapidly enough with increasing wave number to match the experimental data. Consequently, the authors defined an inverse quadratic wave-number-dependent model for the cross-stream turbulence scales, to better capture the measured behavior:

$$\Lambda(k_1) = \left[a\left(k_1 + ck_1{}^2\right) + b\right]^{-1} \tag{9}$$

The constants ($a$, $b$, and $c$) were defined to give a best fit to the discrete empirical scale estimates for the specified separation distances, in the radial and tangential directions, respectively.

In addition to the cross-stream scales, empirical estimates of the streamwise turbulence scales were generated from measured cross-spectral densities by direct inversion of Eq. (6). These data are compared to the fitted radial and tangential scales in Sec. IV.C, to evaluate the fidelity of Taylor's hypothesis.

### B. Large-Scale Circumferential Modes of the Mean Velocity Field

To compute the tangential modes of the mean velocity field at a given radial location, the velocity data must be known over a series of tangential locations, separated by a constant angular step size, over the entire circumference of the circle prescribed by the given radius. Based on these data, the tangential variation of the spatial mean velocity field, $V(R, \phi)$, was defined with respect to the circumferential mean velocity at that radius:

$$V(R, \phi) = U(R, \phi) - \bar{U}^{\phi}(R) \tag{10}$$

The circumferential velocity variations data were measured over a regular annular grid in the rotor inlet plane, as described in Sec. IV.B. These data were used to estimate the discrete circumferential modes of the mean velocity field, using a discrete spatial Fourier transformation to the circumferential domain:

$$\tilde{V}(R_l, n) = \frac{1}{2\pi} \sum_{l=0}^{(N_\phi/2)-1} V(R_l, \phi_n)\, \exp(in\phi_n)\Delta\phi \tag{11}$$

Note that a spatial Hanning window was used to minimize spectral leakage while processing the empirical data presented in Sec. IV.B, but these terms were removed from Eq. (11) for clarity.

## III. Definition of Experiment

### A. Facility

The experiments were performed in the Anechoic Wind Tunnel (AWT) facility at the Hessert Center for Aerospace Research at Notre Dame. This facility is a 61-cm (24-in.) square, freejet, indraft wind tunnel, enclosed in an anechoic chamber. The tunnel has a nominal mean velocity range of 5–33 m/s (17–109 ft/s) and a nominal freestream turbulence intensity at the jet centerline of 0.08% at the inlet exit and 0.2% at the rotor test location. The low-frequency cutoff of the anechoic chamber is approximately 100 Hz. A motorized rotating boom is suspended above the center of the test section, from which microphones can be suspended to measure the far-field acoustic radiation. The current configuration allows accurate acoustic measurements over an arc of approximately 90 deg, centered at the midplane of the test section. Additional information about the AWT facility is given by Mueller et al.[18]

### B. Apparatus

A cylindrical traverse was designed for the cross-stream velocity testing in the propeller inlet plane. This traverse consisted of a Phytron ZSS 42.500 stepper motor, mounted on an aerodynamic stand. It was mounted along the tunnel centerline, on a pair of rails, which enabled continuous variation of the streamwise test location. The stand was designed so that the stepper motor drive axis was coincident with the axis of rotation of the dynamometer. The traverse was used to sweep a pair of single-sensor, hot-wire probes tangentially through the propeller plane, enabling the sensors to sample spatially the incoming velocity field. To ensure statistical significance, the empirical data were ensemble averaged. The turbulence data were then spatially averaged, to approximate the integrating effect of propeller operation. The resulting statistical data were used to define a representive model of the turbulent inflow, as seen by the rotating propeller.

The hot-wire sensors were operated by a TSI IFA100 anemometer, in constant temperature mode. The probes were mounted on radial armatures (Fig. 2), which were attached to the drive axis of the traverse. The mounting armatures permitted continuous variation of the probe separation vector in the propeller plane, in both the radial and/or tangential directions. This system was used to measure the cross spectrum between the fluctuating velocity components from each sensor, for a given sensor separation, at a series of points in the cross-stream plane.

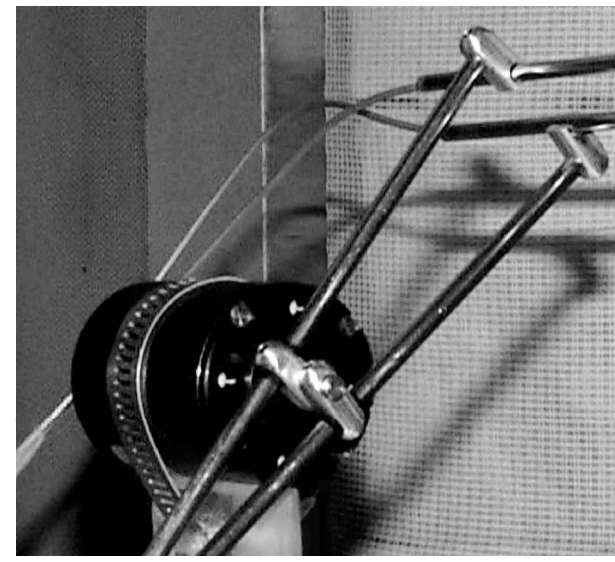

**Fig. 2 Hot-wire mounting armature on cylindrical traverse.**

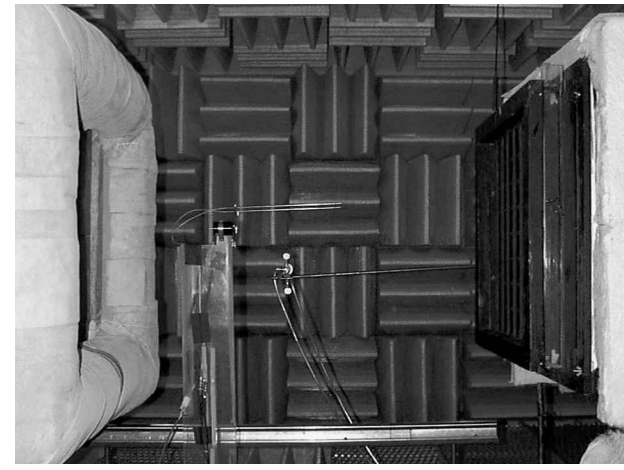

**Fig. 3 Wind-tunnel test configuration shown as configured for velocity testing.**

The tunnel test configuration for the velocity experiments is shown in Fig. 3. As shown in Fig. 3, the turbulence generation grids were mounted upstream of the open test section, in a box attached to the end of the tunnel inlet. The box was designed so that the grids could be changed without altering the test configuration. Three different rectangular grids were used, each with a different mesh spacing, $m = 1.905$, 3.175, and 7.62 cm (0.75, 1.25, and 3.0 in.), and rod diameter, $d = 0.3175$, 0.635, and 1.27 cm (0.125, 0.25, and 0.5 in.), respectively. The resulting grid solidities ($s_{\text{grid}} = 0.26$, 0.34, and 0.33) were nominally equal to those of the grids used by Sevik[1] ($s_{\text{Sevik}} = 0.27$ and 0.34).

### C. Test Conditions

When defining the specific test conditions for the experiments performed in this research project, there were two primary considerations, listed in order of importance: consistency with previous rotor/turbulence ingestion experiments performed at Notre Dame and dynamic similitude with the experimental work of Sevik.[1]

As noted earlier, a great deal of experimental work has been performed at Notre Dame concerning the TIN from a four-bladed rotor.[12,13] The majority of these data were collected at a freestream flow speed of 12.7 m/s (41.9 ft/s). One of the primary objectives of this research project was to perform a detailed empirical assessment of the ingested velocity field, which was only specific to the turbulence generation grid, not the rotor. Because such information

would enhance the utility of the existing empirical response data for the four-bladed rotor at the same speed, a mean flow velocity of 12.7 m/s was selected for the current research. Furthermore, the previous tests of Minniti et al.[13] were taken with the rotor located approximately 61 cm (24 in.) downstream of the grids (measured with respect to the root leading edge of the rotor blades and the trailing edge of the aftmost set of dowels comprising the grids). Because the streamwise location was arbitrary, as long as it was sufficiently far downstream for turbulence to develop, and the AWT test section is fairly short 1.22 m (48 in.), a streamwise rotor location 61 cm (24 in.) downstream of the grids was selected for the current experiments.

A secondary motivation for this research was to investigate possible deficiencies in Sevik's[1] empirical thrust spectrum. The recent theoretical work of Martinez[6–8] suggested that the relative amplitude of the second harmonic of the thrust spectrum should be much lower than that shown in Sevik's published empirical data.[1] However, to make valid comparisons between the two experiments, it was necessary to achieve geometric and dynamic similarity, to the greatest extent possible. Geometric similarity was guaranteed because Sevik's rotor was used in the experiments. To achieve complete dynamic similitude between the two experiments, the following flow parameters had to be matched: the solidity of the turbulence generating grids, the freestream Mach number, the propeller advance ratio, the Reynold's number (based on propeller diameter), the relative amplitude of the velocity disturbance as compared to the freestream flow rate, and the scales of the resulting grid-generated turbulence, relative to the propeller geometry.

As noted earlier, the solidities of the turbulence generation grids used in this study were nominally equivalent to those used by Sevik.[1] Furthermore, the selected freestream velocity of 12.7 m/s (41.9 ft/s) corresponded to a freestream Mach number of approximately 0.01, which was effectively the same as the Mach number achieved in Sevik's experiments ($M \approx 0.03$). In addition, the rotation rate was defined so that the rotor operated at a range of advance ratios ($1.1 \leq J \leq 1.3$), which included that used as in Sevik's experiment ($J_{\text{Sevik}} = 1.22$). Consequently, the first three assumptions listed earlier were satisfied. Because Sevik's experiment was performed in a water tunnel and the current research was performed in air, it was not physically possible to match the Reynold's number. However, this issue was examined by Scharpf, who found that the Reynold's number dependence of the flow through the rotor was weak, so that the flow characteristics in air reflected the behavior in water, as long as there was no cavitation in the water flow.[12] In addition, the rotor was located more than 20 mesh distances downstream of the grids in Sevik's experiments.[1] Such a large separation between the grid and the rotor was not physically possible in the AWT. However, it will be shown in Sec. IV.A that the nominal rms turbulence intensity measured for the given test conditions at the selected rotor streamwise location behind the two larger grids was the same order of magnitude as that measured by Sevik[1] at his test location (≈3%). Thus, the turbulence intensity assumption was also satisfied. The final similarity assumption deals with the relative scales of the ingested turbulence. However, the experimental data presented by Sevik[1] does not include turbulence scales. Given the lack of detailed turbulence scale data, the authors assume that satisfaction of the other similarity assumptions provided a sufficient degree of dynamic similarity between the current experiment and the previous work of Sevik to support valid comparisons between the corresponding results.

The rotor inlet plane was defined to be approximately 61 cm (24 in.) downstream of the grids, which corresponded to the midpoint of the test section. All of the data were taken at a mean freestream velocity of 12.7 m/s (41.9 ft/s), which was the flow speed at which the majority of the previous aeroacoustic response data were taken.[12,13,19]

To ensure statistical significance, all of the measured data were ensemble averaged over a large number of ensembles, each consisting of 2048 samples, collected at a 4-kHz sampling rate. To avoid aliasing high-frequency energy, the data were low-pass filtered at 2 kHz. According to Bendat and Piersol,[20] the required number of data ensembles for sufficient accuracy was smaller for the single-point velocity measurements, such as the mean and rms fluctuation, than the two-point velocity cross spectra used to define the turbulence spatial characteristics. The uncertainties in the measured data were estimated using the error propagation technique of Kline and McClintock (see Ref. 21), as shown in detail by Wojno.[15] Uncertainties of ±2 and ±7% were achieved for the mean and turbulent velocity components, respectively, using 225 data ensembles. In contrast, 625 ensembles were required to provide a nondimensional cross-spectral density resolution of 4%. Below this correlation floor, the measured cross-spectral data must be considered statistically insignificant. The corresponding uncertainty for a 95% statistical confidence level in the measured turbulence cross spectra was ±8% of the measured value.

## IV. Velocity Characterization

To characterize empirically the ingested velocity field, a series of detailed velocity measurements were performed. These tests were performed for all three grids, at a nominal mean flow velocity of 12.7 m/s (41.9 ft/s). Because of space limitations, only the results of the initial turbulence measurements and the streamwise evolution of isotropic turbulence are presented here for all three grids. Detailed characterization of the 7.62-cm grid only, are presented in the remaining sections, because it generated the strongest disturbances. However, similar results were obtained behind the smaller grids.

### A. Initial Velocity Measurements

The first set of experiments were a series of initial velocity tests to measure the rms turbulence intensities upstream of the rotor test location. For these experiments, the sensor was positioned at an arbitrary cross-stream location, approximately 50 cm (20 in.) downstream of each grid. The autospectrum of the turbulence fluctuations were measured behind each grid. The nominal rms turbulence intensities behind each grid were computed based on the autospectra. These data are presented in Table 1.

### B. Spatial Velocity Distribution

The grid of locations at which velocity measurements were taken is shown graphically in Fig. 4. The rotor inlet plane was divided into

**Table 1 Nominal rms turbulence levels measured 50 cm (20 in.) downstream of grid at $U \approx 12.7$ m/s (41.9 ft/s)**

| Mesh size cm (in.) | RMS turbulence velocity, m/s (ft/s) | RMS turbulence intensity, % |
|---|---|---|
| 1.905 (0.75) | 0.37 (1.22) | 2.9 |
| 3.175 (1.25) | 0.53 (1.75) | 4.1 |
| 7.620 (3.00) | 0.79 (2.60) | 6.2 |

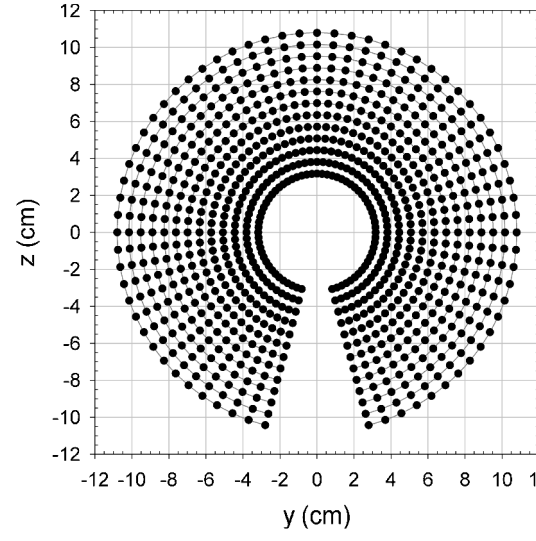


**Fig. 4 Spatial velocity distribution test grid.**

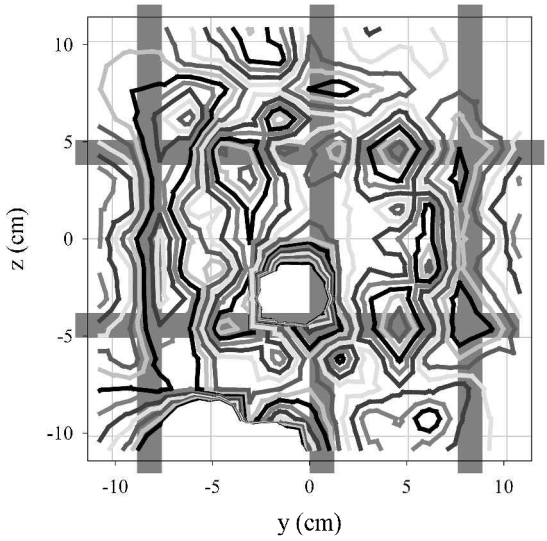


**Fig. 5 Mean velocity structures in rotor inlet plate 61 cm (24 in.) behind downstream of 7.62-cm (3.0-in.) grid.**

a cylindrical test grid, such that $-75 \leq \phi \leq 255$ deg, $\Delta\phi = 5$ deg, $3.175 \leq R \leq 10.795$ cm (4.25 in.), and $\Delta R = 0.635$ cm (0.25 in.).

*Mean Velocity Contours*

A contour plot of the mean velocity distribution is shown in Fig. 5 for the 7.62-cm (3.0-in.) grid. To highlight the spatial correlation with the grid geometry, these data were superimposed on the cross-stream locations of the adjacent upstream rods comprising the grid, indicated in gray. These data clearly demonstrate that the spatial velocity gradients were highly correlated to the relative position of the rods upstream. However, the reader is cautioned against extracting exact velocity values at any location from these plots, because the plotted data were interpolated onto a regular Cartesian grid from the actual measurements that were taken in the cylindrical grid shown in Fig. 4.

*Circumferential Modes of Mean Velocity Field*

As noted earlier, the rotor responds aeroacoustically to circumferential modes of the ingested mean velocity field that are integral multiples of the blade number.[2] The mean velocity contours indicated that the mean velocity field downstream of each of the grids contained some circumferentially varying components. Consequently, the mean velocity distribution was decomposed into its circumferential components. The decomposition was implemented using a spatial DFT.

To compute the tangential modes of the velocity field at a given radial location, the velocity data must be known at a series of tangential locations, separated by a constant angular step size, over the entire circumference of the circle prescribed by the given radius. However, because of mechanical interference between the base of the cylindrical traverse and the armature to which the probes were attached, the experimental data were not collected over the full circumference. Instead, the data were collected over a tangential range of approximately 330 deg (see Fig. 4) because no measurements could be taken over an arc of approximately 30 deg, centered at the base of the traverse. The missing data were filled in with values from measured locations in the upper half of the rotor plane, which were at the same relative position with respect to the adjacent upstream rods comprising the grid. The nominal error from the approximations to the actual velocity data was evaluated by applying the procedure to points adjacent to the missing region, for which measured data were available. Comparisons between the corresponding measured data and the approximation at these locations was less than 1% of the measured value. This error was less than the uncertainty in the measurements themselves, as noted in Sec. III. Consequently, the data approximation technique was deemed sufficiently accurate for this application.

Once the mean velocity data was defined over the entire regular annular grid, the mean velocity distribution was decomposed into its

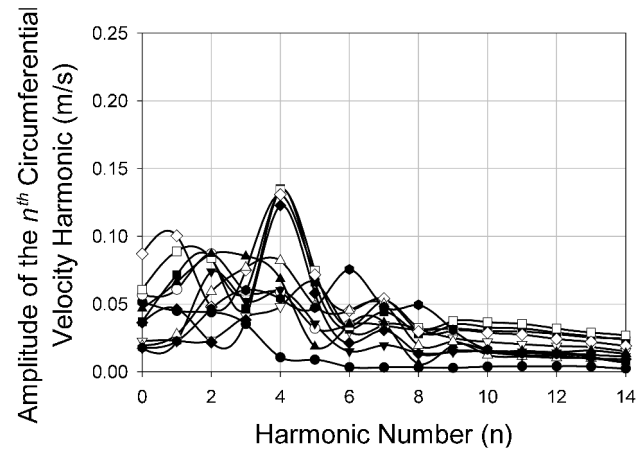


**Fig. 6 Circumferential mean velocity harmonics 61 cm (24 in.) downstream of 7.62-cm (3.0-in.) grid.**

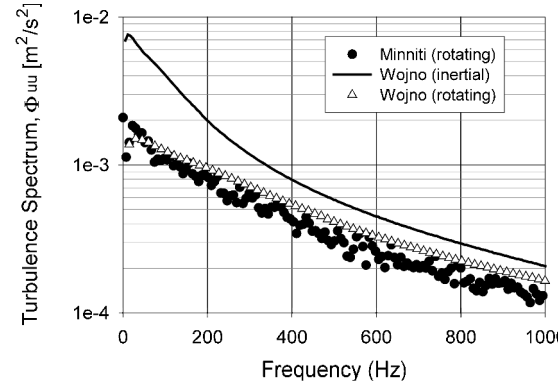


**Fig. 7 Equivalence of turbulence spectra in rotating and inertial reference frames 61 cm (24 in.) downstream of 7.62-cm (3.0-in.) grid.**

circumferential components, using the analysis procedures outlined in Sec. II.B. The results of this analysis are presented in Fig. 6 for the 7.62-cm (3.0-in.) grid. These data indicated that the flow behind the 7.62-cm (3.0-in.) grid included a strong modal component at $n = 4$, but only a weak component at $n = 10$. Consequently, the four-bladed rotor would be expected to generate strong blade passage tones, due to to the circumferentially varying mean velocity field. This behavior was confirmed when the four-bladed rotor response was measured behind this grid.[15] In contrast, the measured acoustic data for the 10-bladed rotor exhibited no strong blade passage tones. Consequently, the apparent modal content indicated for $n = 10$ was deemed insignificant.

### C. Turbulence Characterization

*Velocity Measurement Reference Frame*

Because the cylindrical traverse could not be simultaneously mounted in the AWT with the dynamometer, the velocity measurements had to be performed in an inertial cylindrical reference frame, without the rotor operating in the flow. However, in previous work with the four-bladed rotor, Minniti et al. determined that the streamwise turbulence spectrum, or, equivalently, the temporal turbulence spectrum, is identical in the wave number domain, as long as the appropriate local convection velocity is used.[13] Furthermore, Minniti et al. confirmed that either the rotating or inertial spectra could be used to predict the broadband response of a four-bladed rotor. However, the direct turbulence comparisons that Minniti performed were not published. Only comparisons between the resulting acoustic predictions and the associated measured sound data were presented explicitly. Consequently, Fig. 7 shows a comparison between the turbulence spectrum measured using a rotating sensor behind the 7.62-cm (3-in.) grid (R. J. Minnitti III, private communication) and that measured in this research. When Taylor's hypothesis was used, the inertial data were converted to an equivalent spectrum in the rotating frame, based on the increased convection velocity in

the rotating reference frame, as shown in Eq. (4). These data confirm the equivalence of the turbulence spectra in the rotating and inertial reference frames. In addition, because the rotor was operating at advance ratios close to unity, the acceleration effects of the rotor were deemed to be nominal. Thus, the velocity data presented here were taken in the inertial reference frame, without the rotor operating in the flow.

*Semi-Empirical Spectral Density Model*

As shown in Eq.(1), the directional dependence of the modeled spectral density function was assumed to be separable. This model allowed each spatial direction to be analyzed independently of the others.

*Streamwise Behavior*

The spatially averaged, nondimensional, temporal autospectrum of the turbulent velocity fluctuations measured by each sensor captured the essential behavior of the two-dimensional turbulent wave number spectrum with respect to the temporal frequency. Because the cross-stream direction was arbitrary, this behavior logically extends to the temporal domain and both cross-stream dimensions. However, given Taylor's hypothesis, the temporal frequency and streamwise wave number were equivalent parameters. Consequently, the empirical, temporal autospectrum behind the grid was used to define the streamwise energy content of the semi-empirical, functional three-dimensional turbulence spectral density. As shown in Eq. (1), the streamwise spectral density was nondimensionalized with respect to the mean-squared turbulence fluctuation. The nondimensional streamwise spectral density behind the 7.62-cm (3.0-in.) grid is presented in Fig. 8.

For historical perspective, the measured streamwise spectral density behind the 7.62 cm (3.0 in.) grid was also nondimensionalized in the manner of von Kármán.[22] These data are plotted, along with von Kármán's published data, against the nondimensional streamwise wave number in Fig. 9. For consistency with von Kármán's analysis, the streamwise wave number was nondimensionalized with respect to the wave number of the energy-containing eddies $k_e$ from isotropic flow theory. This parameter was defined as shown in Eq. (12) [Eq. (3–158) in Ref. 15]. A reference line indicating the expected isotropic decay rate, $[k_1/k_e]^{-(5/3)}$, has also been drawn, displaced from the data for clarity:

$$k_e \approx 1.5(u_{\rm rms})^2/\pi E(0) \tag{12}$$

The nondimensional empirical autospectrum measured behind the 7.62-cm (3.0-in.) grid agreed very well with von Kármán's published data.[22] Furthermore, both spectra approach the isotropic trend at high wave numbers.

*Cross-Stream Behavior*

The functional dependence of the three-dimensional wave number spectral density on each of the cross-stream directions (radial or tangential) was determined independently of each other and the streamwise direction. The cross-stream dependence was defined in terms of the theoretical one-dimensional wave number spectral density function given in Eq. (7). Consequently, the spectral density functions in the cross-stream directions were directly dependent on the associated turbulence scales [as shown in Eq. (7)]. However, the scales of the inhomogeneous turbulence field downstream of the grids were actually functions of both position and frequency. An example of the spatial and frequency dependence of the resulting turbulence scale is presented in Fig. 10, which was determined for a fixed tangential probe separation of $\theta = 4$ deg [which corresponded to an arc length $ds = 0.53$ cm (0.21 in.) at the radial probe location $R = 7.62$ cm (3.0 in.)].

These data suggest potential anisotropy of the grid turbulence. For example, the tangential scale exhibited spatial structures, which gave rise to a local banding of the contours, as indicated by the region between the horizontal black lines superimposed in Fig. 10. Similar results were obtained for the radial turbulence scales, although the radial scales at a given temporal frequency were larger (approximately twice as large), and exhibited less spatial structure than the corresponding tangential scales.

However, the overall objective of the analysis was to define a scaled, near-isotropic turbulence model, which was representative of the turbulence characteristics that a blade rotating through the inhomogeneous flow would experience. This model was developed in terms of frequency-dependent turbulence scales [as shown in Eq. (9)], based on circumferentially averaged cross-spectral data, for a number of probe separations. When plotted together, these data defined a general decay trend of the cross-stream turbulence scales with streamwise wave number. The streamwise wave number dependence of the resulting functional representations of the nondimensional radial and tangential turbulence scales is presented, in nondimensional form, in Fig. 11 for the 7.62-cm (3.0-in.) grid. The corresponding empirical coefficients are presented in Table 2.

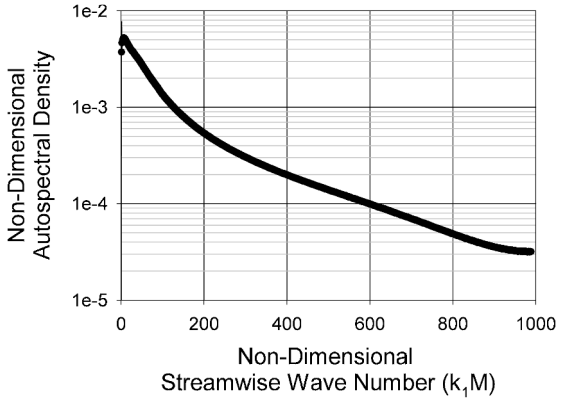


**Fig. 8 Streamwise dependence of turbulence spectral density 61 cm (24 in.) downstream of 7.62-cm (3.0-in.) grid.**

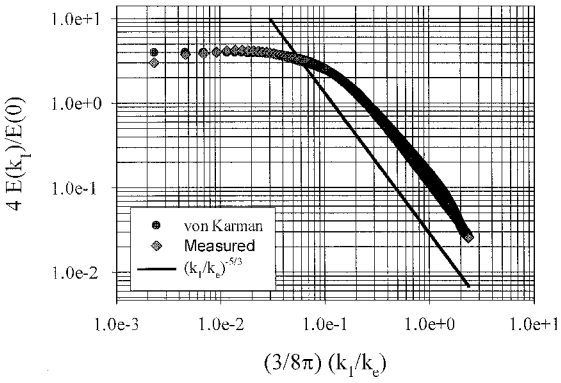


**Fig. 9 Streamwise turbulence spectrum: comparison to historical data 61 cm (24 in.) downstream of 7.62-cm (3.0-in.) grid.**

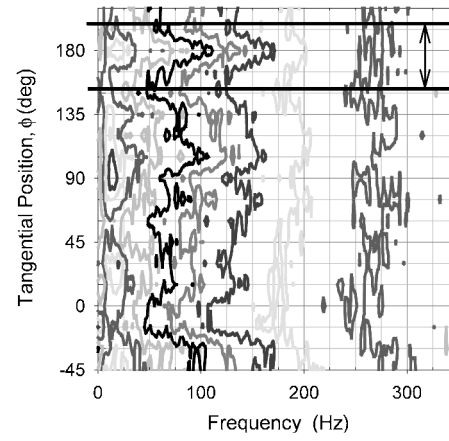


**Fig. 10 Spatial and frequency dependence of tangential turbulence scales 61 cm (24 in.) downstream of 7.62-cm (3.0-in.) grid, probe separation ($r$, $\theta$) = (0.0,4 deg).**

**Table 2 Empirical constants for turbulence scale functions [as defined in Eq. (9)] 61 cm (24 in.) downstream of 7.62-cm (3.0-in.) grid**

| | Empirical constants | | |
|---|---|---|---|
| Direction, $i$ | $a_i$ | $b_i$, $m^{-1}$ | $c_i$, m |
| Tangential | 1.08 | 3.51 | 0.0487 |
| Radial | 0.9 | 0.86 | 0.0487 |

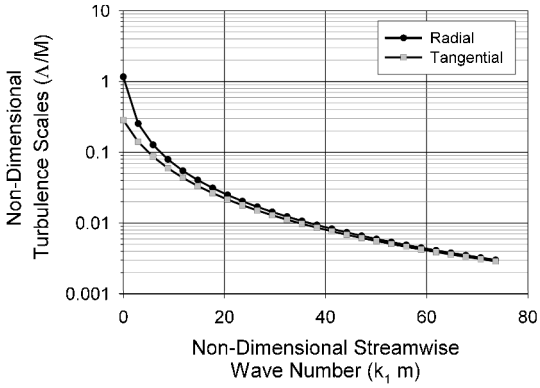


**Fig. 11 Streamwise dependence of empirical turbulence scale functions 61 cm (24 in.) downstream of 7.62-cm (3.0-in.) grid.**

The estimated tangential and radial scales are presented in Fig. 11. These data indicate that both scales were of a comparable order at high wave numbers (or, equivalently, frequency). Furthermore, at the lowest frequencies, the tangential scales were somewhat lower than the corresponding radial scales. However, note that these data were based on the assumed exponential correlation decay presented in Eq. (6), which is primarily valid in the high-frequency limit. Thus, overall, these data support the near isotropy of grid-generated turbulence, which has been documented by numerous previous investigators.[22,23]

Finally, the low-frequency asymptote of the radial turbulence scale, $\Lambda_R$, was ~0.3 mesh spacings, or 2.3 cm (0.9 in.). Because the span of the 10-bladed rotor, $L_R$, was 7.62 cm (3.0 in.), $\Lambda_R/L_R \approx 0.3 < 1$. This relative scaling permitted a simplification of the radial integration, which was required to estimate the unsteady thrust response of the rotor, as shown in part 2 of the TIN research, presented by the authors.[14]

*Evaluation of Taylor's Hypothesis*

The historical criterion for the validity of Taylor's hypothesis is a maximum relative velocity disturbance of approximately 10% of the mean flow rate. This was clearly satisfied by the flow behind each of the grids, as indicated by the measured turbulence intensities listed in Table 1. However, the validity of this assumption was also examined in terms of the relative magnitude of the measured turbulence scales in each spatial direction. Discrete values of the streamwise scales were generated, based on the measured cross-spectral densities, as defined in Eq. (6).

To estimate the streamwise turbulence scales, a series of three velocity cross-spectral measurements were made, with incremental streamwise sensor separation distances. The initial measurement was made for nominally zero streamwise separation. To avoid catastrophic failures due to probe collisions, the sensors were separated in the cross-stream plane by approximately 2.5 mm (0.1 in.). To account for the necessary correlation decay due to even minimal spearations, the zero separation measurement defined the baseline correlation level for these tests. Afterwards, the cross-spectral measurement was repeated twice, with one sensor at the same streamwise location and the other sensor moved 5 cm (2 in.) downstream from the previous test position. These data were used to quantify the correlation decay in the streamwise direction, assuming the following exponential decay model.

As noted earlier, semi-empirical functional models of the radial and tangential turbulence scales were generated based on the discrete empirical data. This was necessary because of the need for a continuous definition of the cross-stream spectral density functions, to evaluate Eq. (1) for arbitrary wave number step sizes. A similar analysis was used on the measured streamwise cross-spectral densities in the Taylor's hypothesis tests. However, the correlation decay in the baseline level, due to the initial sensor displacement in the zero separation configuration, had to be taken into account. This was done by normalizing the nondimensional cross-spectral density over the defined separation, $\gamma(\boldsymbol{x}, f)$, with respect to the baseline value, $\gamma_0(f)$. The resulting ratio was assumed to decay exponentially with streamwise separation as follows:

$$\gamma(\boldsymbol{x}, f)/\gamma_0(f) \approx \exp[-|\boldsymbol{x}|/\Lambda_x(f)] \tag{13}$$

This equation was inverted to obtain discrete estimates of the streamwise turbulence scales, based on the measured cross-spectral densities. The resulting empirical turbulence scale estimates for the 7.62-cm (3.0-in.) grid in all three spatial directions are presented as functions of temporal frequency in Fig. 12. Note that the cross-stream scale values are based on the continuous functional approximation to the discrete measured data. These data demonstrate that the streamwise turbulence scales are orders of magnitude larger than the corresponding cross-stream scales. This result confirms the convection dominance of the flowfield. Consequently, the relative magnitude of the spatial turbulence scales indicates that Taylor's hypothesis is a physically justifiable assumption.

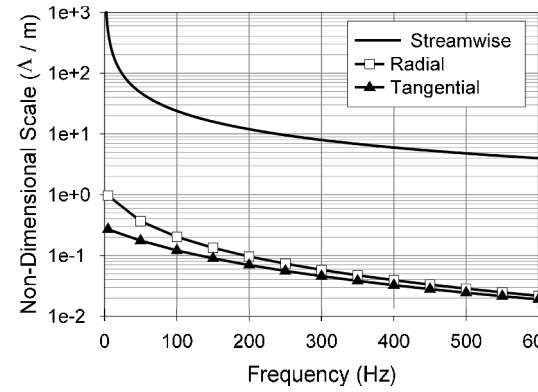


**Fig. 12 Verification of Taylor's hypothesis 61 cm (24 in.) downstream of 7.62-cm (3.0-in.) grid.**

Because Taylor's hypothesis was assessed to be valid, the frequency dependence of the streamwise scales was transformed into a streamwise wave number dependence, as shown in Eq. (2). This was done to obtain a continuous functional approximation to the discrete empirical scale data, in the manner developed in Sec. II.A. Rather than the inverse quadratic wave number dependence demonstrated by the cross-stream scales, however, the inverse linear model developed by Corcos[17] provided a better fit to the empirical streamwise scale data. The value of the empirical coefficient in Eq. (8) that best fit the measured data for the 7.62-cm (3.0-in.) grid was $\hat{a} = \frac{1}{90}$.

*Verification of Separability*

The fundamental assumption used to develop the functional representation of the three-dimensional wave number spectral density in the rotor coordinate system was the assumed separability of the spectral density function [see Eq. (1)]. This assumption simplified the mathematically complex problem of generating a multidimensional surface to describe the behavior of the spectral density function in all three spatial dimensions, that is, streamwise, radial, and tangential, to determine three independent functions that define the behavior of the turbulence in each direction.

As long as Taylor's assumption is valid, the separation of the streamwise behavior from the cross-stream directions was justifiable on physical grounds. It was shown in the preceding section that Taylor's hypothesis was reasonable, based on the relative magnitude of the streamwise and cross-stream scales. In contrast, the separation of the radial and tangential dependence in the rotor plane was incorporated for analytical convenience. To verify the cross-stream directional separability, two-sensor spectral measurements

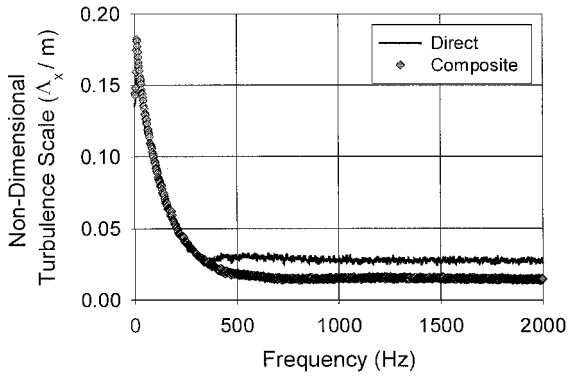


**Fig. 13 Verification of directional separability 61 cm (24 in.) downstream of 7.62-cm (3.0-in.) grid; probe separation $x \equiv (r, \theta) = (0.2$ in. 4 deg).**

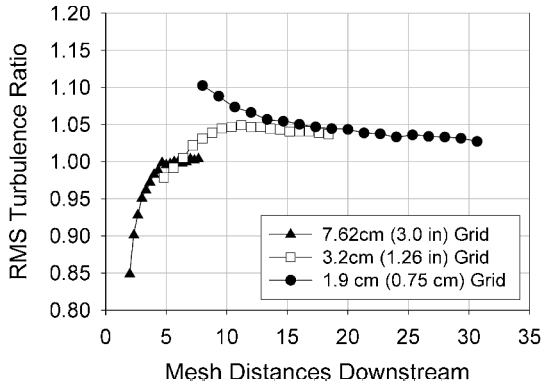


**Fig. 14 Streamwise evolution of isotropy.**

were made for three different separation vectors $\boldsymbol{d}$ at 19 tangential locations in the rotor plane. The separation vectors were defined as the vector sum of component separations in both the radial and tangential directions.

$$\boldsymbol{x} = r\hat{e}_r + R\theta\hat{e}_\theta \tag{14}$$

The temporal cross spectrum between the sensors and the autospectrum measured by each sensor was recorded for each of the defined separation vectors, at each tangential location. These tests were repeated for the corresponding component separations in the radial and tangential directions only. These data were used to estimate the turbulence scales along their respective directions, $\boldsymbol{x}$, $\hat{e}_r$, and $\hat{e}_\theta$. The component scales were combined to generate a theoretical composite scale, assuming a separable, exponentially decaying correlation function. The estimated composite scales were compared to the corresponding measured data to assess the validity of the separability assumption. An example of the measured and composite turbulence scale comparisons is presented in Fig. 13 for $r = 0.2$ in. (5.08 mm) and $\theta = 4$ deg.

These data agreed very well, out to a frequency of approximately 350 Hz. At this frequency, the measured nondimensional turbulence scale levels off at 0.03, whereas the theoretical composite value continues decaying to approximately 0.02 at a frequency of 500 Hz. However, the data beyond 500 and 350 Hz were not statistically significant because they corresponded to measured coherence levels below the minimum resolution of 4%. When these data were disregarded, Fig. 13 demonstrated excellent agreement between the measured and composite turbulence scales. Therefore, these data verify that the assumed directional separability of the three-dimensional turbulent spectral density would successfully capture the relevant flow physics.

*Streamwise Evolution of Isotropy*

Finally, the separability of the turbulence model implied a sort of scaled isotropy, where the streamwise spectral density of the turbulence defined the total energy density of the three-dimensional spectral density function, which was modified by the scale-dependent cross-stream spectral density functions (see Sec. II.A). Consequently, a series of measurements were made to determine the degree of isotropy that existed behind the grid. In particular, the rms turbulence fluctuation was measured using two single-normal hot-wire sensors, which were aligned perpendicular to each other, such that both probe axes were parallel with the streamwise direction. The ratio of the relative turbulence components measured by each sensor provided an estimate of the degree of isotropy. The results of these tests are presented in Fig. 14 for all of the grids. Because this ratio was nominally unity, particularly at the farthest distance downstream of the grids (which was the defined rotor inlet plane), the scaled isotropy model was deemed to be valid.

## V. Conclusions

In this research, a detailed empirical characterization of the ingested grid-generated disturbance field was performed. This velocity field consisted of a spatiotemporally varying turbulence field superimposed on an inhomogeneous mean velocity distribution. A three-dimensional semi-empirical, separable, turbulence model was defined in terms of spatially averaged, measured turbulence characteristics. This separable model was defined using the measured streamwise spectral density (or, equivalently, the temporal autospectral density) of the turbulence and the nondimensional, cross-stream spectral density functions, which were defined in terms of empirical cross-stream turbulence scales. Continuous models for the turbulence scales in each spatial direction were defined as functions of streamwise wave number (or, equivalently, temporal frequency), in the manner of Corcos,[17] using empirically determined constants. The validity of Taylor's hypothesis was verified by the relative amplitudes of these empirical scales, which demonstrated that the streamwise correlation scales were two orders of magnitude larger than the corresponding cross-stream scales. Finally, the measured mean velocity distribution in the rotor inlet plane was shown to exhibit acoustically relevant circumferential modes.

## Acknowledgments

This work was supported by the U.S. Navy, Office of Naval Research, located in Arlington, Virginia, under the following contracts: N00014-97-1-0489, N00014-98-1-0217, and N00014-99-1-0284. The Program Manager was L. Patrick Purtell. This research was performed at the Hessert Center for Aerospace Research, Department of Aerospace and Mechanical Engineering, at the University of Notre Dame.

## References

[1]Sevik, M., "Sound Radiation from a Subsonic Rotor Subjected to Turbulence," NASA SP-304, 1971.

[2]Blake, W., *Mechanics of Flow Induced Sound and Vibration*, Wiley, New York, 1986, Chap. 12.

[3]Lighthill, M., "On Sound Generated Aerodynamically I: General Theory," *Proceedings of the Royal Society of London*, Vol. A221, 1952, pp. 564–587.

[4]Lighthill, M., "On Sound Generated Aerodynamically II: Turbulence as a Source of Sound," *Proceedings of the Royal Society of London*, Vol. A222, 1954, pp. 1–32.

[5]Martinez, R., and Weissman, K., "Spatial-Domain Analysis of the Thrust on a Propeller Cutting Through Isotropic Turbulence," Cambridge Acoustics Associates, CAA Rept. U-1894-358.47, Cambridge, MA, Dec. 1990.

[6]Martinez, R., "Asymptotic Theory of Broadband Rotor Thrust, Part I: Manipulations of Flow Probabilities for a High Number of Blades," *Journal of Applied Mechanics*, Vol. 63, March 1996, pp. 136–142.

[7]Martinez, R., "Asymptotic Theory of Broadband Rotor Thrust, Part II: Analysis of the Right Frequency Shift of the Maximum Response, *Journal of Applied Mechanics*, Vol. 63, March 1996, pp. 136–142.

[8]Martinez, R., "Broadband Sources of Structure-Borne Noise for Propulsors in Haystacked Turbulence," *Computers and Structures*, Vol. 65, No. 30, 1995, pp. 475–490.

[9]Paterson, R. W., and Amiet, R. K., "Acoustic Radiation and Surface Pressure Characteriscics of an Airfoil Due to Incident Turbulence," NASA CR-2733, 1976.

[10]Manoha, E., "Broadband Noise from a Propeller in Turbulent Flow," *Proceedings of the ASME, Noise Control and Acoustics Division*, NCA Vol. 25, American Society of Mechanical Engineers, Fairfield, NJ, 1998.

[11]Ffowcs-Williams, J. E., and Hawkings, D. L., "Sound Generation by Turbulence and Surfaces in Arbitrary Motion," *Philosophical Transactions*

*of the Royal Society of London, Series A: Mathematical and Physical Sciences*, Vol. 264, No. 1151, 1969, pp. 321–342.

[12]Scharpf, D. F., "An Experimental Investigation of the Sources of Propeller Noise Due to Turbulence Ingestion," Ph.D. Dissertation, Dept. of Aerospace and Mechanical Engineering, Univ. of Notre Dame, Notre Dame, IN, Jan. 1993.

[13]Minniti, R. J., III, Blake, W. K., and Mueller, T. J., "Determination of Inflow Distortion Characteristics by Interpreting the Aeroacoustic Response of a Propeller Fan," *Proceedings of the 4th AIAA/CEAS Aeroacoustics Conference*, Vol. 1, Confederation of European Aerospace Societies, Toulouse, France, 1998, pp. 483–496.

[14]Wojno, J. P., Mueller, T. J., and Blake, W. K., "Turbulence Ingestion Noise, Part 2: Rotor Aeroacoustic Response to Grid-Generated Turbulence," *AIAA Journal*, Vol. 40, No. 1, 2002, pp. 26–32.

[15]Wojno, J. P., "An Experimental Investigation of the Aeroacoustic Response of a Ten-Bladed Rotor Ingesting Grid-Generated Turbulence," Ph.D. Dissertation, Dept. of Aerospace and Mechanical Engineering, Univ. of Notre Dame, Notre Dame, IN, April 1999.

[16]Hinze, J. O., *Turbulence*, McGraw-Hill, New York, 1975.

[17]Corcos, G. M., "The Structure of the Turbulent Pressure Field in Boundary-Layer Flows," *Journal of Fluid Mechanics*, Vol. 18, 1964, pp. 353–378.

[18]Mueller, T. J., Scharpf, D. F., Batill, S. M., Strebinger, R. B., Sullivan, C. J., and Subramanian, S., "The Design of a Low-Noise, Low-Turbulence Wind Tunnel for Acoustic Measurements," AIAA Paper 92-3883, 1992.

[19]Subramanian, S., "Experimental and Computational Studies on Propeller Noise Due to Inflow Distortion," Ph.D. Dissertation, Dept. of Aerospace and Mechanical Engineering, Univ. of Notre Dame, Notre Dame, IN, May 1993.

[20]Bendat, J., and Piersol, A. G., *Random Data: Analysis and Measurement Procedures*, Wiley, New York, 1986, p. 368.

[21]Figliola, R., and Beasley, D. E., *Theory and Design for Mechanical Measurements*, Wiley, New York, 1991, p. 150.

[22]von Kármán, T., "Progress in the Statistical Theory of Turbulence," *Journal of Marine Research*, Vol. 7, No. 3, 1948, pp. 252–264.

[23]Dryden, H. L., "Turbulence Investigations at the National Bureau of Standards," *Proceedings of the 5th International Congress of Applied Mechanics*, Wiley, New York, 1939, pp. 362–368.

P. J. Morris
*Associate Editor*